Measurement of the quantum states of squeezed light

G. Breitenbach, S. Schiller & J. Mlynek

Fakultät für Physik, Universität Konstanz, D-78457 Konstanz, Germany

A state of a quantum-mechanical system is completely described by a density matrix or a phase-space distribution such as the Wigner function. The complete family of squeezed states of light (states that have less uncertainty in one observable than does the vacuum state) have been generated using an optical parametric amplifier, and their density matrices and Wigner functions have been reconstructed from measurements of the quantum statistics of their electric fields.

A central theme in many fields of quantum physics is the development and application of theoretical and experimental tools for obtaining information about the states of quantum fields of matter and radiation. Although the state of an individual particle or system is unobservable, it is possible to determine the state of an ensemble of identically prepared systems by performing a large number of measurements[1]. Notable experimental succcess has recently been achieved in generating and determining states of various quantum-mechanical systems, employing newly developed methods of quantum state reconstruction (QSR)[2–9]. A single mode of light[10–14], vibrational modes of a diatomic molecule[15] and of an ion in a Paul trap[16], and the motional state of freely propagating atoms[17] have been characterized completely by determining their density matrix or, equivalently, their Wigner functions, a quantum-mechanical analogue of the classical phase-space distribution[18].

A single spatial monochromatic mode of light represents a harmonic oscillator system for which non-classical states can be generated very efficiently using the interaction of laser light with nonlinear optical media. Squeezed states[19], first generated about ten years ago[20,21], have a reduced uncertainty in a specific quadrature (for example the amplitude quadrature) compared to that of the vacuum state. They have typically been characterized by measuring the variances of the electric field with a homodyne detector. A complete investigation of their quantum features, in particular their photon statistics (which at present cannot be measured directly owing to technical limitations of available photon counters) has only become possible through the recent development of theoretical tools for QSR. First experimental investigations analysed coherent and squeezed vacuum states[10,11,13,14]. Here we present a study of all types of squeezed states of light; squeezed vacuum, amplitude-squeezed states, phase-squeezed states and states squeezed in an arbitrary quadrature. For each of these states we construct 'portraits' in terms of both the Wigner functions (which are two-dimensional maps in appropriate phase-space coordinates) and the density matrices. These portraits contain all that one can know about the quantum-mechanical properties of the squeezed optical states.

Optical homodyne tomography

How is the quantum state of an optical wave determined? The measurements to be performed on the state are measurements of the electric field operator $E(\theta) \propto X_\theta = X\cos\theta + Y\sin\theta$ at all phase angles θ. Here $X = (a + a^\dagger)/\sqrt{2}$, $Y = (a - a^\dagger)/\sqrt{2}i$ are the non-commuting quadrature operators of the electric field, with a and $a^\dagger$ being the annihilation and creation operators. X and Y are analogous to position and momentum operators of a particle in a harmonic potential. To access experimentally the electric field, which oscillates with a frequency of $\omega/2\pi$ of hundreds of THz, a balanced homodyne detector[22] is employed (see Fig. 1). In this detector, the signal wave is spatially overlapped at a beamsplitter with a local-oscillator wave of the same frequency. The two fields emerging from the beamsplitter are proportional to the sum and the difference of the signal and local-oscillator fields. By detecting the difference of their fluxes, the natural oscillation of the signal state under investigation is converted to a low-frequency electrical signal i_-, which measures X_θ, where θ is the relative phase between signal and local oscillator. A large number of measurements of the observable X_θ yields the probability distribution $P_\theta(x_\theta)$ of its eigenvalues x_θ. This procedure is repeated for a set of different phase angles $\theta \in [0, \pi]$.

The relation between the measured distributions and the density operator ρ is $P_\theta(x_\theta) = \langle x \mid U^\dagger(\theta)\rho U(\theta) \mid x \rangle$, where $U(\theta) = \exp(-i\theta a^\dagger a)$ performs a rotation in phase space. As the optical state evolves freely with ω, U is equivalent to the time evolution operator with $\theta = \omega t +$ constant, and the θ-dependence of P_θ is equivalent to the time dependence of the position probability density of the state (that is, of $|\psi(x,t)|^2$, if $\rho = |\psi\rangle\langle\psi|$ is a pure state). Thus, homodyne detection maps out the time evolution of a harmonic oscillator state. Our measurements (shown below) may be regarded as an implementation of the oldest example of quantum dynamics, the motion of a wavepacket in a harmonic potential studied by Schrödinger in 1926[23].

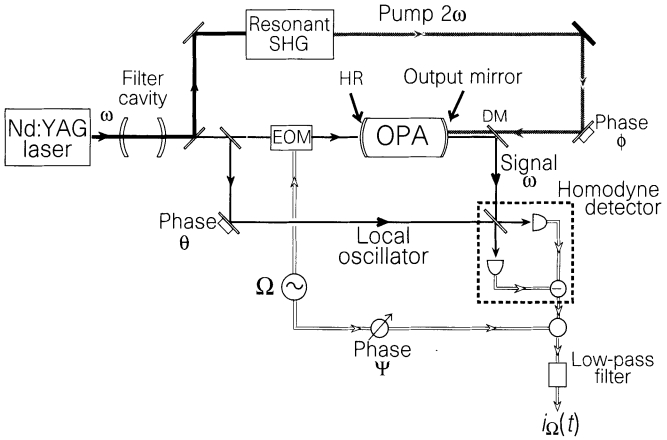

Figure 1 Experimental scheme for generating bright squeezed light and squeezed vacuum with an optical parametric oscillator (OPA). The electric field quadratures are measured in the homodyne detector while scanning the phase θ. A computer performs the statistical analysis of the photocurrent i_Ω and reconstructs the quantum states. EOM, electro-optic modulator; DM, dichroic mirror; SHG, second harmonic generator; HR, high reflector.

Of the various methods that have been proposed to reconstruct the quantum state numerically from the set of measured distributions P_θ, two are employed here. The first method makes use of the fact that the distributions $P_\theta(x_\theta)$ are the marginals of the Wigner function $W(x, y)$ in rotated coordinates;

$$P_\theta(x_\theta) = \int_{-\infty}^{\infty} W(x_\theta \cos\theta - y_\theta \sin\theta, x_\theta \sin\theta + y_\theta \cos\theta)\, \mathrm{d}y_\theta \qquad (1)$$

where $y_\theta = -x \sin\theta + y \cos\theta$. Therefore $W(x, y)$ can be obtained from the set P_θ by back-projection via the inverse Radon transform[2]. The second method furnishes the elements of the density matrix in the Fock basis via integration of the distributions P_θ over a set of pattern functions[3,4]. In contrast to the inverse Radon transform, this procedure does not involve any filtering of the experimental data and also allows an estimation of the propagation of statistical errors.

The experiment

The experimental set-up is shown in Fig. 1. Central to the experiment is a monolithic standing-wave lithium-niobate optical parametric oscillator (OPA)[13,24], pumped by a frequency-doubled continuous-wave Nd:YAG laser (1,064 nm). The infrared laser wave is filtered by a high-finesse mode-cleaning cavity, which transmits 75% of the laser power. Its narrow linewidth of 170 kHz suppresses the high-frequency technical noise of the laser, yielding a shot-noise-limited local oscillator for light powers in the milliwatt range at frequencies ⩾1 MHz (ref. 13). The pump wave 2ω (power ~20–30 mW) for the OPA is generated by resonant second harmonic generation.

In the past OPAs have been frequently used as sources of non-classical light[10,13,25–28]. Operated below threshold, the OPA is a source of squeezed vacuum. We studied the field's spectral compnents around a frequency offset by $\Omega/2\pi = 1.5$ or 2.5 MHz from the optical frequency ω, to avoid low-frequency laser excess noise. To generate bright light (that is, with non-vanishing average electric field at the frequencies $\omega \pm \Omega$), we employ the OPA in a dual port configuration[28]. A very weak wave split off the main laser beam is phase-modulated by an electro-optic modulator (EOM) at the frequency Ω (modulation index $\beta \ll 1$) and injected into the

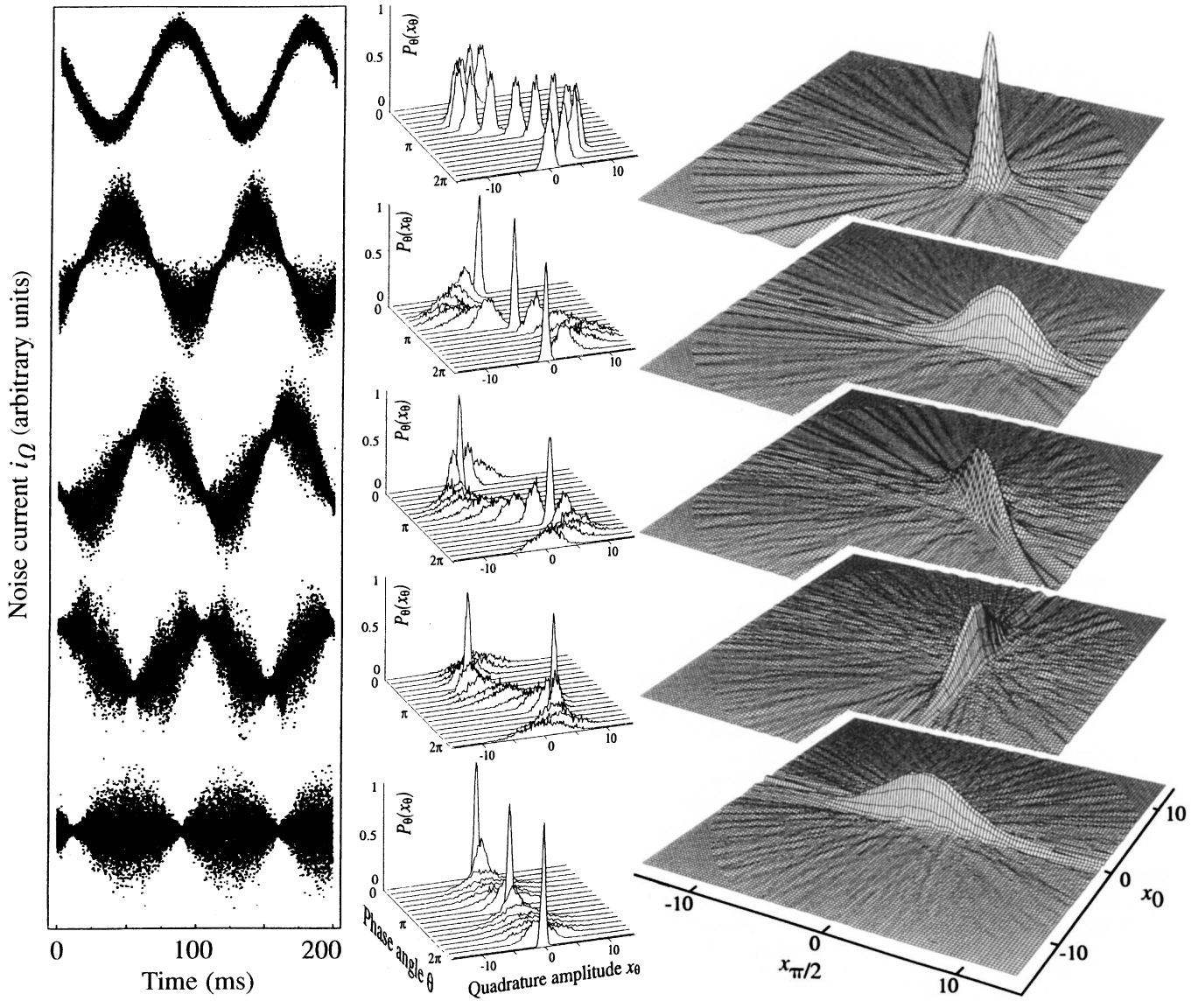

Figure 2 Noise traces in $i_\Omega(t)$ (left), quadrature distributions $P_\theta(x_\theta)$ (centre), and reconstructed Wigner functions (right) of generated quantum states. From the top: Coherent state, phase-squeezed state, state squeezed in the $\phi = 48°$-quadrature, amplitude-squeezed state, squeezed vacuum state. The noise traces as a function of time show the electric fields' oscillation in a 4π interval for the upper four states, whereas for the squeezed vacuum (belonging to a different set of measurements) a 3π interval is shown. The quadrature distributions (centre) can be interpreted as the time evolution of wave packets (position probability densities) during one oscillation period. For the reconstruction of the quantum states a π interval suffices.

OPA through its high reflector (HR) port. The carrier frequency ω is kept on-resonance with the cavity and the two 'bright' sidebands $\omega \pm \Omega$ are well within the cavity bandwidth $\Gamma/2\pi = 17$ MHz (HWHM). In the semiclassical picture we may write the Fourier components at the frequency Ω' of the field's quadratures emitted from the output mirror as $X(\Omega') = E_0(\Omega') + \beta E_0(\delta(\Omega' - \Omega) - \delta(\Omega' + \Omega)) + X_n(\Omega')$, $Y(\Omega') = Y_n(\Omega')$, where δ is the Dirac delta-function, E_0 is the amplitude of the emitted wave and X_n, Y_n are the broad-band quantum fluctuations[29]. Due to the very small ratio of HR transmission (<0.1%) to output mirror transmission (2.1%), the transmitted sidebands and their quantum fluctuations are strongly attenuated. The quantum fluctuations of the signal wave inside the resonator originate essentially from the vacuum fluctuations entering through the output coupler. The injected seed-wave amplitude as well as the fluctuations are modified inside the resonator by the interaction with the 2ω pump wave: the quadrature fluctuations out-of-phase with the pump are deamplified (squeezed), the in-phase quadrature fluctuations are amplified. Similarly, the seed wave is deamplified if it is out of phase, and amplified if it is in phase, with the pump wave. As the relative phase ϕ between seed wave and pump wave is controlled manually by a mirror attached to a piezoelectric actuator, deamplified amplitude-squeezed light, amplified phase-squeezed light and light squeezed in an arbitrary quadrature are easily generated. The coherent excitation of the sidebands is controlled coarsely by changing the power of the seed wave (the photon flux of the carrier E_0 at the OPA output port is about 6×10^8 photons $s^{-1} = 120$ pW), fine control is achieved by varying the modulation strength of the EOM. By turning the modulation off, we obtain squeezed vacuum, which has been described in detail previously[13,14]. By blocking the OPA pump wave, we are left with coherent states.

The signal is analysed at a homodyne detector, whose output current i_- is mixed with an electrical local oscillator $\sim\sin(\Omega t + \phi)$ phase-locked to the modulation frequency, and then low-pass filtered with 100 kHz bandwidth. We fix the phase of the electric local oscillator to $\cos\phi = 1$, so that the resulting current is;

$$i_\Omega(\theta, t) = (2\beta E_0 + X_n(\Omega, t) - X_n(-\Omega, t))\sin\theta + (Y_n(\Omega, t) - (Y_n(-\Omega, t))\cos\theta \quad (2)$$

where $X_n(\Omega, t)$, $Y_n(\Omega, t)$ are the noise fluctuations in a 100-kHz-wide band centred at Ω. By variation of the optical local-oscillator phase θ, any quadrature of the field difference at $\omega + \Omega$ and $\omega - \Omega$ can be accessed.

The i_Ω data (about 500,000 points per trace) are taken with a high-speed 12 bit analogue-to-digital converter, while the local-oscillator phase is swept by 2π in approximately 200 ms. Time traces of i_Ω for coherent and squeezed states are shown in the left column of Fig. 2. They can be considered to be the experimental counterpart of the theoretical depictions of squeezed states introduced by Caves[30].

The traces are subdivided into 128 equal-duration intervals within which the local-oscillator phase is approximately constant. These individual time traces may be regarded as the quantum trajectories of a particular quadrature X_θ. The specific behaviour of the trajectory is unpredictable; its statistics however contain the information necessary and sufficient to calculate the quantum state properties. Experimentally, the statistics are obtained by forming histograms of 256 amplitude bins for each quantum trajectory and normalizing the absolute bin width using as reference the distribution of a vacuum state. The middle column of Fig. 2 shows selected measured quadrature probability distributions for the generated states. All distributions are found to be gaussians. This is expected, as the states are generated from a coherent state with a gaussian Wigner function via a second-order nonlinear interaction.

The variances of these distributions determine the amount of squeezing and anti-squeezing. A maximum of -6 ± 0.25 dB

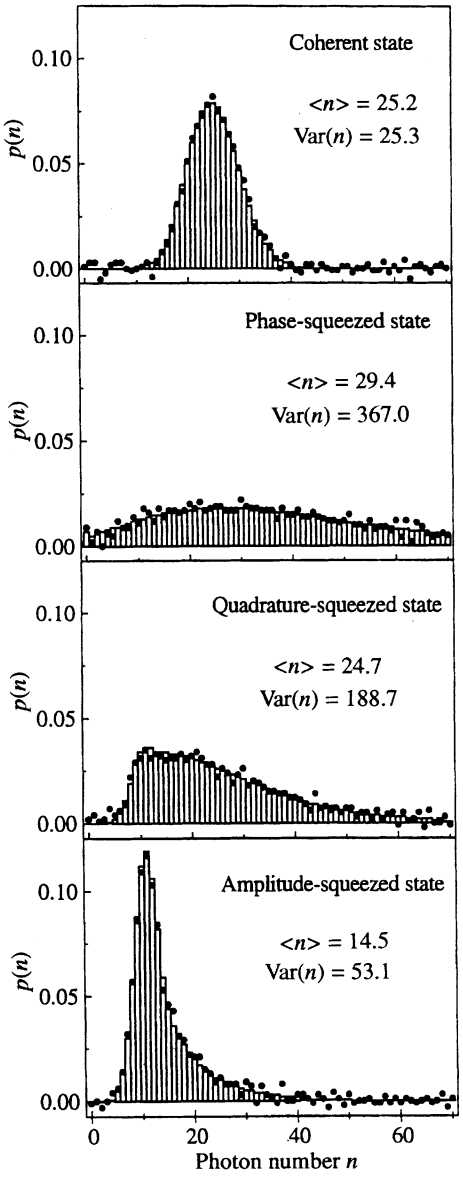

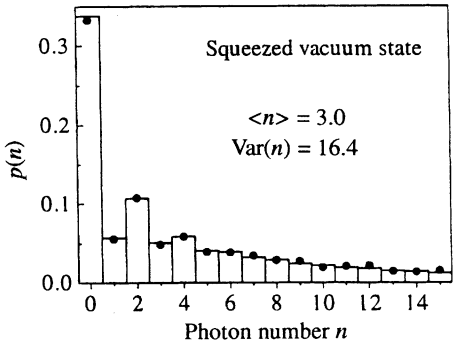

Figure 3 Photon number distributions for the states of Fig. 2. Solid points refer to experimental data, histograms to theoretical expectations. Except for the poissonian distribution of the coherent state, all distributions are super-poissonian ($\langle n \rangle < \mathrm{Var}(n)$). The odd/even oscillations in the photon number distribution of the squeezed vacuum state are a consequence of the pair-wise generation of photons. They can also be explained by quantum interference effects in phase space[37].

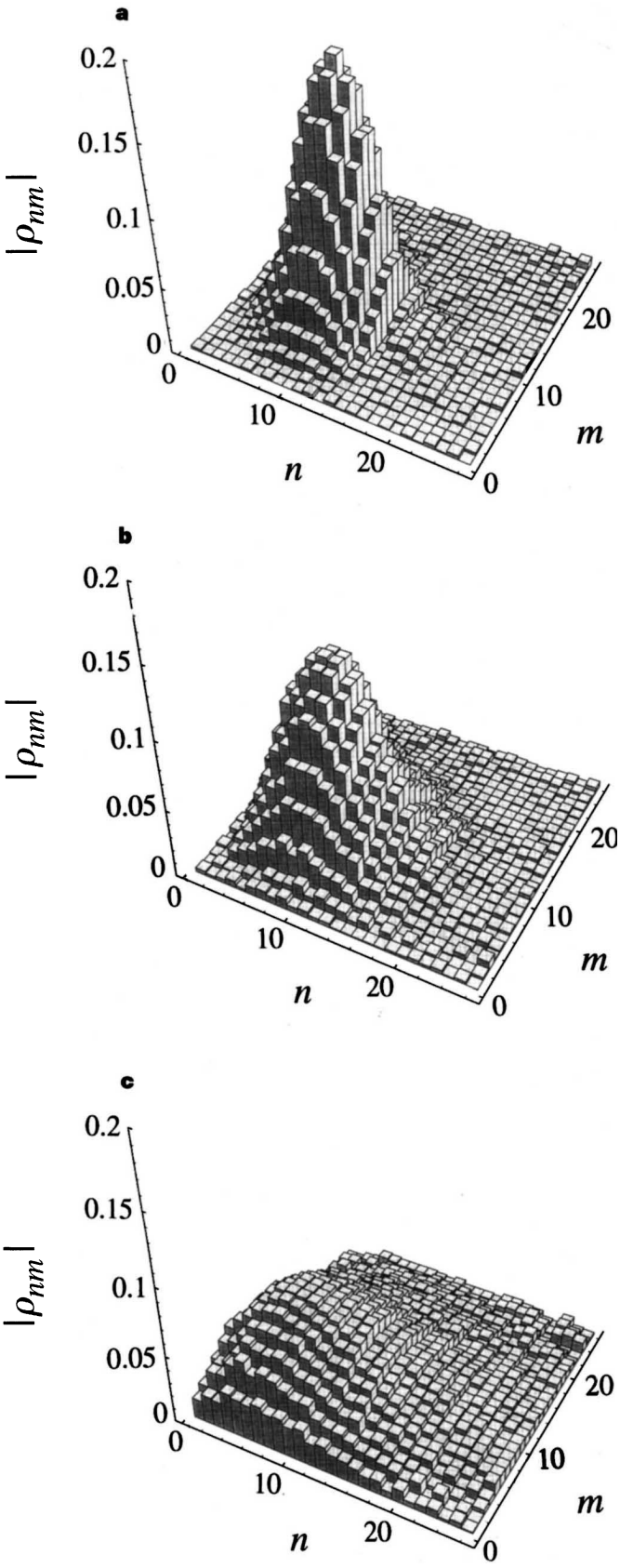

Figure 4 Reconstructed density matrices (absolute values) of three states with approximately equal amplitude: **a**, sub-poissonian amplitude-squeezed state with $\langle n\rangle = 8.9$, $\mathrm{Var}(n) = 4.9$; **b**, coherent state with $\langle n\rangle = 8.4$, $\mathrm{Var}(n) = 8.6$; **c**, phase-squeezed state with $\langle n\rangle = 8.4$, $\mathrm{Var}(n) = 24.6$. The bump around $n \approx 17, m \approx 12$ for the amplitude-squeezed state is a characteristic feature, where the matrix elements change sign.

(= 0.25) for the squeezed vacuum mode was detected. For the bright squeezed light only a maximum amount of squeezing of − 5.2 dB (= 0.3) was reached, due to slight phase instabilities of the seed wave. The anti-squeezing amounted to 12–14 dB (= 15.8–26.9) for the states presented. These values agree with the results of simultaneous measurements with a spectrum analyser.

Phase-space distributions of squeezed states

Applying the inverse Radon transform yields the Wigner distributions shown in the right column of Fig. 2. They agree well with the theoretical expression;

$$W(x,y) = \frac{1}{\pi ab}\exp\left(-\frac{(x-e_0\cos\phi)^2}{a^2} - \frac{(y-e_0\sin\phi)^2}{b^2}\right) \quad (3)$$

where $x = x_0\cos\phi + x_{\pi/2}\sin\phi$, $y = -x_0\sin\phi + x_{\pi/2}\cos\phi$ are the phase-space coordinates used in standard textbooks, a and b are respectively the minimum and maximum standard deviation of the quadrature fluctuations, and $e_0 = 2\beta E_0$ is the state's amplitude. The commonly used depiction of squeezed states as ellipses in phase space, with half-axes a and b, corresponds to a horizontal section through the Wigner function. The area of the ellipse is a measure of the purity of the state, as $\mathrm{Tr}\rho^2 = 2\pi\int\int W(x,y)^2\mathrm{d}x\mathrm{d}y$ equals $1/ab$ for squeezed states (here Tr indicates the trace of a matrix). $\mathrm{Tr}\rho^2$ amounted to 1 for the (pure) coherent state and 0.41–0.46 for the squeezed states of Fig. 2. Their significantly mixed character arises mostly from loss experienced in the cavity of the OPA (escape efficiency 0.88) and during propagation and detection (overall detection efficiency $\eta = 0.94$).

The quantum efficiency of the detection system is a critical issue in the field of QSR[31]. The loss suffered by the quantum state in propagation and detection is equivalent to a convolution of its original Wigner function with a gaussian. Thus for a given detection efficiency η only the s-parametrized phase-space distribution function $W(x, y, s)$ (ref. 18) with $s < 1 - (1/\eta)$, can be reconstructed[32]. In a strict sense the Wigner function itself $W(x, y) = W(x, y, s = 0)$ is not accessible by tomographical methods, but with our high detection efficiency our reconstructions yield phase-space distributions with $s = -0.064$, which is very close to the Wigner function. An additional smoothing, also a convolution with a gaussian, occurs within the reconstruction algorithm in a filtering procedure with a quadratic regularization method[33]. However, its contribution to the total s-parameter can be made less than − 0.01.

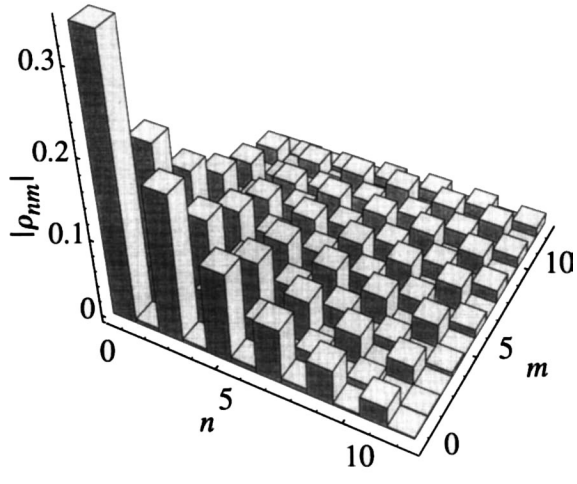

Figure 5 Reconstructed density matrix of the squeezed vacuum state of Fig. 2: along the diagonal and the near off-diagonals the elements alternate in magnitude, which can be explained by quantum interference in phase space[37]. Odd off-diagonals are zero, owing to the symmetry of the state's distribution in phase space, $W(x,y) = W(-x, -y)$.

Density matrices of squeezed states

An alternative view of the generated states is provided by their density matrices ρ in the Fock basis, because here the state is described in terms of energy eigenstates, in contrast to the description by field components discussed in the previous paragraph. The diagonal elements of the density matrix $\rho_{nn} = p(n)$, are the occupation probabilities of the number states $|n\rangle$. Here n is to be interpreted as the photon flux per unit bandwidth; $p(n)$ is the probability that an ideal photon counter would register in 1 second n photons in a 1-Hz-wide spectral band. A state with $\langle n\rangle$ photons corresponds to a photon flux of $\langle n\rangle \times 10^5$ photons $s^{-1} \approx \langle n\rangle 0.02$ pW in the 100-kHz-wide spectral bands centred at $\omega \pm \Omega$.

Figure 3 shows the photon number distributions for the states from Fig. 2. As can be seen, a simple rotation of the squeezing ellipse (with respect to the coherent excitation in phase space) changes the photon distribution function substantially. Apart from the poissonian distribution of the coherent state, all distributions shown are strongly super-poissonian, that is, the photon number variance $\mathrm{Var}(n)$ exceeds its mean $\langle n\rangle$. For amplitude-squeezed light this seems counterintuitive, as reduced amplitude noise should imply reduced intensity (photon number) noise. An explanation is given by the expressions for photon number average and variance for general (non-minimum-uncertainty) squeezed states[34]:

$$\langle n\rangle = \frac{1}{4}(a^2 + b^2 - 2) + \frac{1}{2}e_0^2$$
$$\mathrm{Var}(n) = \frac{1}{8}(a^4 + b^4 - 2) + \frac{1}{2}e_0^2(a^2\cos^2\phi + b^2\sin^2\phi) \quad (4)$$

For states with a large amplitude e_0, the variance of the amplitude quadrature $a^2\cos^2\phi + b^2\sin^2\phi$ indeed determines the characteristics of the photon number distribution. However, in the regime of low amplitudes, when coherent excitation and quantum noise are comparable in size, the first terms in equation (4), figuratively the photon content of the quadrature fluctuations, play a significant role. We adjusted the experimental parameters to $a^2 = 0.43$, $b^2 = 3.3$ (reduced squeezing and anti-squeezing) and $e_0 = 4.12$ to obtain amplitude-squeezed sub-poissonian light. Its Mandel-Q-parameter $(\mathrm{Var}(n) - \langle n\rangle)/\langle n\rangle = -0.45$ is to our knowledge the lowest value achieved so far using optical nonlinear frequency-conversion techniques[35].

Figure 4 shows the density matrix up to $n, m = 25$ for the sub-poissonian amplitude-squeezed state in comparison with those of a coherent and super-poissonian phase-squeezed state with approximately equal average photon numbers. Owing to their reflection symmetry in phase space, it is always possible to choose a basis in which the density matrices of these three states in the Fock representation are real. For the coherent state and the phase-squeezed state all elements ρ_{nm} are positive, for the amplitude-squeezed state the near-diagonals show oscillations. The density matrix of the squeezed vacuum, Fig. 5, exhibits the most interesting structure. Its typical 'chess-board' pattern is due to the down-conversion process occurring in the OPA, where photons are created in pairs. The deviations of the experimental density matrices presented here from the theoretical ones are of the order of 0.01 per element. Besides statistical effects, this is partly due to instabilities of the relative phases θ and ϕ and to fluctuations in the pump power.

We have carried out a complete experimental characterization of the whole family of squeezed states. Average photon number and orientation of the states in phase space were accurately controlled by macroscopic experimental parameters. In particular, this flexibility allowed us to generate amplitude-squeezed light with either sub- or super-poissonian photon statistics. The quantum state reconstructions were performed in quasi real-time, with a data acquisition time of 200 ms and an analysing time of ~20 s. Our results are in very good agreement with theory. Beyond the reconstructions presented here, we have investigated the Pegg–Barnett phase distribution and incoherent superpositions of coherent states[36].

Quantum state reconstruction by homodyne tomography has been developed into a reliable and accurate tool. We believe that this powerful method will stimulate experimental efforts to generate new quantum states with non-gaussian statistics using higher-order nonlinear processes. □

Received 10 January; accepted 15 April 1997.

1. Royer, A. Measurement of quantum states and the Wigner function. *Foundat. Phys.* **19,** 3–32 (1989).
2. Vogel, K. & Risken, H. Determination of quasiprobability distributions in terms of probability distributions for the rotated quadrature phase. *Phys. Rev. A* **40,** 2847–2849 (1989).
3. D'Ariano, G. M., Macchiavello, C. & Paris, M. G. A. Detection of the density matrix through optical homodyne tomography without filtered back projection. *Phys. Rev. A* **50,** 4298–4302 (1994).
4. Leonhardt, U., Munroe, M., Kiss, T., Richter, Th. & Raymer, M. G. Sampling of photon statistics and density matrix using homodyne detection. *Opt. Commun.* **127,** 144–160 (1996).
5. Leonhardt, U. & Raymer, M. G. Observation of moving wave packets reveals their quantum state. *Phys. Rev. Lett.* **76,** 1985–1989 (1996).
6. Richter, T. & Wünsche, A. Determination of occupation probabilities from time-averaged position distributions. *Phys. Rev. A* **53,** R1974–R1977 (1996).
7. Zucchetti, A., Vogel, W., Tasche, M. & Welsch, D.-G. Direct sampling of density matrices in field-strength bases. *Phys. Rev. A* **54,** 1–4 (1966).
8. Banaszek, K. & Wodkiewicz, K. Direct probing of quantum phase space by photon counting. *Phys. Rev. Lett.* **76,** 4344–4347 (1996).
9. Tan, S. M. An inverse problem approach to optical homodyne tomography. (spec. iss. on QSR) *J. Mod. Opt.* (submitted).
10. Smithey, D. T., Beck, M., Raymer, M. G. & Faridani, A. Measurement of the Wigner distribution and the density matrix of a light mode using optical homodyne tomography: application to squeezed states and the vacuum. *Phys. Rev. Lett.* **70,** 1244–1247 (1993).
11. Smithey, D. T., Beck, M., Cooper, J. & Raymer, M. G. Measurement of number-phase uncertainty relations of optical fields. *Phys. Rev. A* **48,** 3159–3167 (1993).
12. Munroe, M., Boggavarapu, D., Anderson, M. E. & Raymer, M. G. Photon number statistics from the phase-averaged quadrature field distribution: theory and ultrafast measurement. *Phys. Rev. A* **52,** R924–R927 (1995).
13. Breitenbach, G. *et al.* Squeezed vacuum from a monolithic optical parametric oscillator. *J. Opt. Soc. Am. B* **12,** 2304–2309 (1995).
14. Schiller, S., Breitenbach, G., Pereira, S. F., Müller, T. & Mlynek, J. Quantum statistics of the squeezed vacuum by measurement of the density matrix in the number state representation. *Phys. Rev. Lett.* **77,** 2933–2936 (1996).
15. Dunn, T. J., Sweetser, J. N. & Walmsley, I. A. Experimental determination of the quantum-mechanical state of a molecular vibrational mode using fluorescence tomography. *Phys. Rev. Lett.* **74,** 884–887 (1995).
16. Leibfried, D. *et al.* Experimental determination of the motional quantum state of a trapped atom. *Phys. Rev. Lett.* **77,** 4821–4285 (1996).
17. Kurtsiefer, C., Pfau, T. & Mlynek, J. Measurement of the Wigner function of an ensemble of helium atoms. *Nature* **386,** 150–153 (1997).
18. Hillery, M., O'Connell, R. F., Scully, M. O. & Wigner, E. P. Distribution functions in physics: fundamentals. *Phys. Rep.* **106,** 122–167 (1984).
19. Walls, D. Squeezed states of light. *Nature* **306,** 141–146 (1983).
20. Slusher, R. E., Hollberg, L. W., Yurke, B., Mertz, J. C. & Valley, J. F. Observation of squeezed states generated by four wave mixing in an optical cavity. *Phys. Rev. Lett.* **55,** 2409–2412 (1985).
21. Kimble, H. J. & Walls, D. F. (eds) (spec. iss. on squeezing light) *J. Opt. Soc. Am. B* **4(10),** (1987).
22. Yuen, H. P. & Chan, V. W. S. Noise in homodyne and heterodyne detection. *Opt. Lett.* **18,** 177–179 (1983).
23. Schrödinger, E. Der stetige Übergang von der Mikro- zur Makromechanik. *Naturwissenschaften* **14,** 664–666 (1926).
24. Breitenbach, G., Schiller, S. & Mlynek, J. 81% conversion efficiency in frequency-stable continuous-wave parametric oscillation. *J. Opt. Soc. Am. B* **12,** 2095–2101 (1995).
25. Wu, L.-A., Kimble, H. J., Hall, J. L. & Wu, H. Generation of squeezed states by parametric down conversion. *Phys. Rev. Lett.* **57,** 2520–2523 (1986).
26. Polzik, E. S., Carri, J. & Kimble, H. J. Spectroscopy with squeezed light. *Phys. Rev. Lett.* **68,** 3020–3023 (1992).
27. Kim, C. & Kumar, P. Quadrature-squeezed light detection using a self-generated matched local oscillator. *Phys. Rev. Lett.* **73,** 1605–1608 (1994).
28. Schneider, K., Bruckmeier, R., Hansen, H., Schiller, S. & Mlynek, J. Bright squeezed light generation by a continuous-wave semi-monolithic parametric amplifier. *Opt. Lett.* **21,** 1396–1397 (1996).
29. Collett, M. J. & Walls, D. F. Squeezing spectra for nonlinear optical systems. *Phys. Rev. A* **32,** 2887–2892 (1985).
30. Caves, C. M. Quantum limits on noise in linear amplifiers. *Phys. Rev. D* **26,** 1817–1839 (1982).
31. D'Ariano, G. M., Leonhardt, U. & Paul, H. Homodyne detection of the density matrix of the radiation field. *Phys. Rev. A* **52,** R1801–R1804 (1995).
32. Leonhardt, U. & Paul, H. Realistic optical homodyne measurements and quasiprobability distributions. *Phys. Rev. A* **48,** 4598–4604 (1993).
33. Janicke, U. & Wilkens, M. Tomography of atom beams. *J. Mod. Opt.* **42,** 2183–2199 (1995).
34. Dodonev, V. V., Man'ko, O. V. & Man'ko, V. I. Photon distribution for one-mode mixed light with a generic gaussian Wigner function. *Phys. Rev. A* **49,** 2993–3001 (1994).
35. Davidovich, L. Sub-Poissonian processes in quantum optics. *Rev. Mod. Phys.* **68,** 127–172 (1996).
36. Breitenbach, G. & Schiller, S. Homodyne tomography of classical and non-classical light. (spec. iss. on QSR) *J. Mod. Opt.* (submitted).
37. Schleich, W. & Wheeler, J. A. Oscillations in photon number distribution of squeezed states and interference in phase space. *Nature* **326,** 574–577 (1987).

Acknowledgements. We thank T. Müller and S. F. Pereira for their collaboration in the initial stage of the experiment, and A. Faridani and M. G. Raymer for providing the source code for the inverse Radon Transform. We also thank R. Bruckmeier, U. Leonhardt, W. P. Schleich, G. M. D'Ariano and S. M. Tan for discussions. This work was supported by the Deutsche Forschungsgemeinschaft and the EC Esprit programme.

Correspondence and requests for materials should be addressed to G.B. (e-mail: Gerd.Breitenbach@uni-konstanz.de). A video showing the time evolution of the quantum states presented here can be obtained from the authors.